bioRxiv preprint doi: https://doi.org/10.1101/043869; this version posted March 15, 2016. The copyright holder for this preprint (which was not certified by peer review) is the author/funder, who has granted bioRxiv a license to display the preprint in perpetuity. It is made available under aCC-BY-NC 4.0 International license.

Left-right leaf asymmetry in decussate and distichous phyllotactic systems

Ciera C. Martinez*[,1], Daniel H. Chitwood*[,2], Richard S. Smith[3,4], Neelima R. Sinha[#,5]

*These authors contributed equally.

[1]Dept. of Molecular & Cell Biology, University of California, Berkeley, Berkeley, CA 94720 USA.

[2]Donald Danforth Plant Science Center, St. Louis, MO 63132 USA.

[3]Department of Comparative Development and Genetics, Max Planck Institute for Plant Breeding Research, Cologne, 50829 Germany.

[4]Institute of Plant Sciences, University of Bern, CH-3013 Bern, Switzerland

[5]Department of Plant Biology, University of California, Davis, Davis, CA 95616 USA.

KEYWORDS: Plant development, symmetry, auxin, phyllotaxy, leaf development, phyllotaxy

[#]To whom correspondence should be addressed:

Neelima R. Sinha

Department of Plant Biology

1002 Life Sciences

One Shields Ave.

Phone: (530) 754-8441

Fax: (530) 752-5410

e-mail: nrsinha @ ucdavis.edu

bioRxiv preprint doi: https://doi.org/10.1101/043869; this version posted March 15, 2016. The copyright holder for this preprint (which was not certified by peer review) is the author/funder, who has granted bioRxiv a license to display the preprint in perpetuity. It is made available under aCC-BY-NC 4.0 International license.

ABSTRACT

Leaves in plants with spiral phyllotaxy exhibit directional asymmetries, such that all the leaves originating from a meristem of a particular chirality are similarly asymmetric relative to each other. Models of auxin flux capable of recapitulating spiral phyllotaxis predict handed auxin asymmetries in initiating leaf primordia with empirically verifiable effects on superficially bilaterally symmetric leaves. Here, we extend a similar analysis of leaf asymmetry to decussate and distichous phyllotaxy. We found that our simulation models of these two patterns predicted mirrored asymmetries in auxin distribution in leaf primordia pairs. To empirically verify the morphological consequences of asymmetric auxin distribution, we analyzed the morphology of a tomato *sister-of-pinformed1a* (*sopin1a*) mutant, *entire-2*, in which spiral phyllotaxy consistently transitions to a decussate state. Shifts in the displacement of leaflets on the left and right sides of *entire-2* leaf pairs mirror each other, corroborating predicted model results. We then analyze the shape of >800 common ivy (*Hedera helix*) and >3,000 grapevine (*Vitis* and *Ampelopsis* spp.) leaf pairs and find statistical enrichment of predicted mirrored asymmetries. Our results demonstrate that left-right auxin asymmetries in models of decussate and distichous phyllotaxy successfully predict mirrored asymmetric leaf morphologies in superficially symmetric leaves.

INTRODUCTION

Leaf shape is defined across four axes. Asymmetry is usually obvious along three of these axes—the proximal-distal, abaxial-adaxial, and medio-lateral (**Figure 1A**), while asymmetry along a fourth axis, which describes the left and right halves of a leaf (**Figure 1B**), is rarely explored. Most leaves are thought to be either truly bilaterally symmetric (i.e., each side of the leaf mirrored along the midrib) or if asymmetry is observed, on average this asymmetry cancels

bioRxiv preprint doi: https://doi.org/10.1101/043869; this version posted March 15, 2016. The copyright holder for this preprint (which was not certified by peer review) is the author/funder, who has granted bioRxiv a license to display the preprint in perpetuity. It is made available under aCC-BY-NC 4.0 International license.

59 out. Fluctuating asymmetry observed along the left/right axis of leaves has been attributed to
60 noise created from random errors during development, influenced by environmental stresses [1–
61 3]. Random noise in development can be assumed if the average difference between the left and
62 right sides is zero, but if there is a consistent shift in asymmetry on one side compared to the
63 other, directionalized asymmetry may be occurring [4].
64
65 Recent work using sensitive techniques to measure leaf shape has suggested that directionalized
66 asymmetry along the left and right side of the leaf may be more prevalent than once believed.
67 Although superficially bilaterally symmetric, Elliptical Fourier Descriptor analysis in
68 *Arabidopsis thaliana*, in addition to simple measurements in the shifts between leaflet placement
69 along the left and right sides of *Solanum lycopersicum* (tomato) leaves, reveals that plants in
70 these species produce leaves biased to be left- or right-handed [5]. The asymmetry of leaves is
71 dependent on the handedness of the plant from which they originate. Handedness in plants arises
72 when the phyllotaxy (the angular arrangement of initiated leaves and other lateral organs on a
73 plant) is spiral (i.e., the angle between initiating leaves is approximately the golden angle,
74 ~137.5°). In reference to a "bottom-up" view of leaf initiation events, the spiral can form in two
75 directions, either "clockwise" (C) or "counter-clockwise" (CC) (**Figure 1C**). The observation
76 that leaf morphological features are asymmetrically skewed in relation to spiral phyllotactic
77 patterning has been described in exceptionally asymmetric species with respect to features such
78 as venation patterning, leaf shape, curling, coiling, and resupination [6, 7]. Notably, many of the
79 examples in the previous references are from the Zingiberales, including banana (*Musa*) and
80 *Calathea*, reported to have a fixed phyllotactic handedness [7, 8]. The left and right sides of a
81 leaf in plants with spiral phyllotaxy therefore appear to possess intrinsic asymmetries influenced

bioRxiv preprint doi: https://doi.org/10.1101/043869; this version posted March 15, 2016. The copyright holder for this preprint (which was not certified by peer review) is the author/funder, who has granted bioRxiv a license to display the preprint in perpetuity. It is made available under aCC-BY-NC 4.0 International license.

by whether the phyllotaxy of the plant is clockwise or counter-clockwise (**Figure 1C**). To reflect the orientation of a leaf relative to the spiral phyllotactic direction, various terminologies have been proposed [7, 9–11]. In this paper, the leaf half which faces towards emerging leaves will be described as ascending, while the half facing the older leaves is the descending side (**Figure 1C**).

Modeling and experimental approaches have shown that phyllotactic patterning is largely determined by the localization of the plant hormone auxin [12, 13]. Regions of high auxin concentration determine sites of leaf initiation and the positional information of many other leaf features during morphogenesis, including vasculature, leaflets, and the development of the margin [14, 15]. The dynamics of auxin flux in spiral phyllotactic systems are such that it is predicted that auxin would be depleted from the ascending side of older primordia and supplied to the descending side of younger primordia. This prediction was verified both in existing auxin flux models of the shoot apical meristem (that have provided foundational insights into the self-organizing mechanisms by which auxin flux creates phyllotactic patterns) and empirically, by looking at the asymmetric shape features of initiating and mature leaves and the distribution of auxin reporter activity in leaf primordia [5]. While leaf asymmetry is guided by biased auxin distribution during spiral phyllotactic patterning, no one has explored how leaf asymmetries manifest in plants which display other phyllotactic patterns.

While the most common phyllotactic pattern in the plant kingdom is spiral, phyllotaxy can take on a multitude of orientations, including decussate and distichous. In decussate patterns pairs of leaves initiate at the same time 180° apart with subsequent leaf pares initiating at 90° from previous pair (**Figure 1E**). Distichous phyllotaxy is similar except leaves initiate one at a time, at a divergence angle of 180° (**Figure 1F**). In spiral systems the left-right axis is fixed and the

bioRxiv preprint doi: https://doi.org/10.1101/043869; this version posted March 15, 2016. The copyright holder for this preprint (which was not certified by peer review) is the author/funder, who has granted bioRxiv a license to display the preprint in perpetuity. It is made available under aCC-BY-NC 4.0 International license.

106 developmental context of each side of a primordium depends on phyllotactic chirality, but in
107 decussate and distichous phyllotaxy, the potential relationship between asymmetry in leaves
108 relates to their initiation as pairs.
109
110 To explore the asymmetric nature of leaves arising from decussate and distichous systems, we
111 asked if leaf asymmetries exist using both modeling and empirical approaches. We first revisited
112 an auxin flux model that is capable of recapitulating decussate and distichous phyllotaxy. We
113 found that there are predicted auxin asymmetries in initiating decussate and distichous leaf
114 primordia pairs (that is, the divergence angle between the pair is ~180°) such that auxin falls on
115 opposite sides of each leaf. Curious if such a mirrored relationship is empirically supported, we
116 took advantage of a recently characterized *sister-of-pin-formed1a* (*sopin1a*) mutant in tomato,
117 *entire-2* (*e-2*), that displays a consistent decussate phyllotaxy at early nodes [16]. Leaf pairs in *e-*
118 *2* exhibit mirrored shifts in the displacement of leaflets on the left and right sides of the leaf,
119 verifying modeled predictions. We then analyze the morphology of >800 distichous leaf pairs
120 using Elliptical Fourier Descriptors in common ivy (*Hedera helix*) and find a statistical
121 enrichment for successive leaves to have opposite asymmetry above that expected by chance. A
122 similar analysis using homologous Procrustes-adjusted landmarks in >3,000 leaf pairs from 20
123 different species and hybrids of grapevine (*Vitis* and *Ampelopsis* spp.) shows that the predicted
124 mirrored asymmetries in successive leaves are particularly strong in this group. Our results show
125 that even in decussate and distichous species seemingly lacking directional asymmetries, models
126 of asymmetric auxin flux successfully predict left-right asymmetries in mature leaves.
127
128 RESULTS

bioRxiv preprint doi: https://doi.org/10.1101/043869; this version posted March 15, 2016. The copyright holder for this preprint (which was not certified by peer review) is the author/funder, who has granted bioRxiv a license to display the preprint in perpetuity. It is made available under aCC-BY-NC 4.0 International license.

129 **Modeling predicts mirrored IAA shifts between pairs of leaves in decussate and distichous**
130 **phyllotaxy**

131 Previous work asked if there are differences in auxin localization with respect to initiating leaf
132 primordia using models capable of simulating spiral phyllotactic patterning [5]. We re-visit this
133 model, which is capable of predicting many phyllotactic patterns, including spiral, decussate, and
134 distichous [13]. The model works by simulating known mechanisms that direct leaf initiation
135 events. The simulation reiterates through several steps. 1. Directional auxin transport by the
136 action of the auxin efflux transporter, PIN-FORMED1 (PIN1), which directs auxin towards
137 neighboring cells with the highest auxin concentration. 2. Auxin accumulates to convergence
138 points. 3. Once auxin levels reach a certain threshold, auxin is transported inward beginning leaf
139 initiation on the periphery of the simulated shoot apical meristem (SAM). Unlike the spiral and
140 decussate models, in the distichous model the original equations from Smith and co-workers are
141 stable enough to be used such that original transport equations, rather than those assuming no
142 primordium differentiation, are used without *PIN* polarity bias in primordium cells. Thus our
143 methods here are independent of the particular choice of transport equation, as several have been
144 proposed [13, 17, 18].
145
146 The analysis of decussate and distichous systems is different from spiral phyllotaxis, as pairs of
147 primordia are analyzed for relationships between their divergence angles and IAA Shift values.
148 For the decussate system, a pair of leaves has to be preceded by a divergence angle between 70°
149 and 100°, and the pair itself requires a divergence angle >150°. In the distichous system, a "pair"
150 of leaves consists of two successive leaves in which the divergence angle is >130°. To facilitate
151 analysis, divergence angles were converted to a positive sign that forces a similar orientation in

bioRxiv preprint doi: https://doi.org/10.1101/043869; this version posted March 15, 2016. The copyright holder for this preprint (which was not certified by peer review) is the author/funder, who has granted bioRxiv a license to display the preprint in perpetuity. It is made available under aCC-BY-NC 4.0 International license.

all leaf primordia pairs. We then analyzed the relationships between divergence angles and IAA Shift values (the deviation of the center of mass of auxin distribution in a leaf primordium relative to the divergence angle) between "primordium A" and "primordium B" (see **Figure 2A**). If IAA Shift values between a pair of distichous or decussate primordia are of the same sign (e.g. shifting clockwise in both primordia, or counter-clockwise in both primordia) then we expect auxin maxima to fall on the same side of each primordium such that they are of a "pinwheel" orientation (**Figure 2B**). Contrastingly, if the IAA Shift values between primordium A and B are opposite in sign, the auxin maxima fall on mirroring sides of a primordia pair, forming a "mirror" orientation (**Figure 2C**). In both decussate and distichous models, we find that IAA Shifts form a mirroring pattern within primordia pairs (**Figure 2D-F**). In primordium A, as the divergence angle decreases from the ideal 180˚, IAA Shift values decrease and become negative, whereas in primordium B as the divergence angle decreases, IAA Shift values increase and become significantly positive. The results show that as decussate or distichous pairs of leaves deviate from an ideal 180˚ divergence angle the auxin peak concentrations remain truer to 180˚, creating mirror image pairs of primordia as in (**Figure 2C**) that is often empirically observed, as in distichous arrangements of *Begonia* leaves (**Figure 2G**).

Decussate *e-2* tomato plants display mirrored asymmetries in leaflet position but not terminal leaflet shape

We investigated if auxin asymmetries observed in the decussate model had empirical consequences for leaf morphology in a tomato mutant. Ideally, hypotheses regarding the effects of different phyllotactic systems would not be made between disparate species (such as tomato and *Begonia*) but within a single species. Although mutations that create aberrant phyllotaxis are

bioRxiv preprint doi: https://doi.org/10.1101/043869; this version posted March 15, 2016. The copyright holder for this preprint (which was not certified by peer review) is the author/funder, who has granted bioRxiv a license to display the preprint in perpetuity. It is made available under aCC-BY-NC 4.0 International license.

176 commonplace, those that produce true transformations from one stable phyllotactic patterning
177 form to another are exceedingly rare [19]. We took advantage of the *e-2* mutation, which has
178 been shown to display decussate-like phyllotaxis, where the divergence angle between leaves 1
179 and 2 and leaves 3 and 4 approaches 180°, but the angle between leaves 2 and 3 is much smaller
180 (**Figure 3A-B**) [16].
181
182 In our previous study [5], the displacement of leaflet position between the left and right sides of
183 the tomato compound leaf was a strong indicator of asymmetry and predicted auxin distributions
184 from the spiral phyllotactic model. For those decussate pairs formed from the first two leaves for
185 which there were leaflets to measure (n=113), we measured the difference in distance from the
186 terminal leaflet to the first distal lateral leaflet between the left and right side of *e-2* leaves
187 (**Figure 3C**). The direction of the asymmetry of the displacement of leaflets was strongly
188 opposite and mirrored between leaves 1 and 2 in *e-2*, which form a divergence angle greater than
189 that found in wild-type and closer to 180˚ (**Figure 3B**). The correlation between the left-right
190 displacement in leaves 1 and 2 in *e-2* is strongly negative ($r = -0.51$, $p = 8 \times 10^{-9}$, n=113) (**Figure**
191 **3D**), confirming the mirrored relationship between pairs predicted by modeling (**Figure 2D**), and
192 distinctly different from the leaflet displacement in the same direction common to leaves arising
193 from wild-type tomato plants with spiral phyllotaxy as we have shown previously [5].
194
195 In our previous work on spiral phyllotaxy, we had analyzed terminal leaflet shapes using
196 Elliptical Fourier Descriptors (EFD) and found that leaves arising from plants of a particular
197 handedness were asymmetric in a similar direction. Analyzing leaf1/leaf2 pairs in *e-2*, we asked
198 whether an opposite orientation in asymmetric leaflet shape occurred more frequently than a
199 similar orientation by chance (**Figure 4A**), as predicted by the "mirrored" orientation observed in

bioRxiv preprint doi: https://doi.org/10.1101/043869; this version posted March 15, 2016. The copyright holder for this preprint (which was not certified by peer review) is the author/funder, who has granted bioRxiv a license to display the preprint in perpetuity. It is made available under aCC-BY-NC 4.0 International license.

our model (**Figure 2D**). To do so, we isolated the asymmetric sources of EFD variance (**Figure 4B**) and asked how often each resulting Principal Component (PC) was of the opposite or same sign between leaf1/leaf2 pairs in *e-2*. A one-tailed Fisher's exact test (in the direction of the alternative hypothesis of more opposite pairs relative to same, assuming equal numbers) fails to achieve significance, leaving the modeled hypothesis of mirrored asymmetry unconfirmed with respect to terminal leaflet shape (**Table 1**).

The mirrored relationship in terminal leaflet pairs may have failed to achieve significance for any number of reasons, including a subtle effect not detected because of insufficient replication (n = 183, which is small compared to the replication measured for common ivy or grapevine species, see below) or that directionalized asymmetry may only be observed in leaflet displacement (**Figure 3D**) and not terminal leaflet shape. This last hypothesis is intriguing, considering that for all PCs, more same orientations were observed than opposite (**Table 1**). Considering that tomato is a spiral phyllotactic species and that this is a mutant, perhaps the spiral-phyllotactic tendency for terminal leaflet asymmetries to be of the same sign [5] is preserved in an *e-2* genetic background. Regardless, the mirrored displacements in leaflet position (**Figure 3C-D**) are predictive of the modeled mirror relationship (**Figure 2D**) and distinct from what we had previously observed in leaflet position in a wild type background [5], suggesting that some leaf features are affected more by the *e-2* decussate transformation than others.

Alternating leaf asymmetry in the distichous phyllotaxy of common ivy (*Hedera helix*) and grapevine (*Vitis* and *Ampelopsis* spp.)

bioRxiv preprint doi: https://doi.org/10.1101/043869; this version posted March 15, 2016. The copyright holder for this preprint (which was not certified by peer review) is the author/funder, who has granted bioRxiv a license to display the preprint in perpetuity. It is made available under aCC-BY-NC 4.0 International license.

222 To test whether the modeled mirrored predictions for distichous phyllotaxy (**Figure 2F**) are
223 empirically observable, we turned to distichous vine species, which present numerous numbers
224 of paired, successive nodes to test our hypotheses.
225
226 We analyzed 824 leaf pairs of a single genotype of common ivy (*Hedera helix*) growing up a
227 >6m concrete wall enclosing a courtyard at the Donald Danforth Plant Science Center in St.
228 Louis, MO (**Figure 5A**). Asymmetric shape variance was quantified using Elliptical Fourier
229 Descriptors (EFDs) (**Figure 5B**). For the first four asymmetric Principal Components (PCs)
230 explaining 87.5% of asymmetric shape variance, more opposite than same signed relationships
231 were detected between leaf pairs (**Table 2**). However, only for PCs 2 and 3 was the occurrence
232 of opposite-signed leaf pairs significantly greater than that of same-signed pairs at a p value less
233 than the α level of 0.05 using a one-way Fisher's exact test (**Table 2**). We conclude that
234 especially for specific asymmetric leaf features (defined by PCs 2 and 3 in this particular case)
235 the distichous phyllotactic condition in common ivy confers an alternating, mirrored asymmetry
236 to successive leaves, as predicted by modeling (**Figure 2F**).
237
238 Next, we analyzed >3,000 leaf pairs from 20 different *Vitis* and *Ampelopsis* species and hybrids
239 from a germplasm collection maintained by the USDA in Geneva, NY (USA). This previously
240 published dataset [20] analyzed leaf shape in >270 vines by collecting all the leaves from a
241 single shoot and recording their order (**Figure 5C**). Using 17 homologous landmarks
242 superimposed using a Procrustes analysis, both symmetric and asymmetric sources of shape
243 variance are analyzed, but asymmetry is almost exclusively restricted to a specific Principal
244 Component (PC), in this case PC4 which explains 10.5% of the total shape variance (**Figure**
245 **5D**). Performing a one-way Fisher's exact test to determine if successive leaf pairs with opposite

bioRxiv preprint doi: https://doi.org/10.1101/043869; this version posted March 15, 2016. The copyright holder for this preprint (which was not certified by peer review) is the author/funder, who has granted bioRxiv a license to display the preprint in perpetuity. It is made available under aCC-BY-NC 4.0 International license.

246 PC4 signs are more prevalent than same-signed pairs, reveals a strong enrichment of mirrored,
247 asymmetric leaf pairs across numerous *Vitis* and *Ampelopsis* species and some hybrids (**Table 3**).
248 Our results demonstrate that although not necessarily apparent at first glance, grapevine and
249 related species exhibit strong alternating asymmetries in successive leaves (**Figure 5C-D; Table**
250 **3**) consistent with the predictions from models of auxin flux in distichous systems (**Figure 2F**).
251
252 DISCUSSION
253 Although they are strikingly different patterning events, our results elucidate common themes
254 between the asymmetries that arise in spiral, decussate, and distichous phyllotaxis (**Figure 6**). In
255 spiral systems, the peak auxin concentration is displaced towards the descending side of the
256 center of mass of leaf primordia, resulting in a distal shift of morphological features (including
257 leaflet placement and terminal leaflet shape) in mature leaves. The distal shift of morphological
258 features is observed empirically in leaf primordia that lunge towards the ascending side due to
259 increased growth along their descending edge (**Figure 6A**) [5], reminiscent of the curvatures
260 seen in more extremely asymmetric leaved species, such as leaf shape in *Calathea* or the
261 positioning of serrations in holly [7, 21]. A similar scenario occurs in decussate and distichous
262 systems, except that deviation in divergence angles creates angles less than 180° that, when
263 accompanied by shifts in auxin peak concentrations that remain truer to 180°, creates mirrored
264 morphologies in leaf pairs (**Figure 2F; Figure 6B-D**). The mirrored relationship between leaf
265 pairs is strikingly observed in the left-right displacement of leaflets in the leaves of the decussate
266 tomato mutant *entire-2* (**Figure 3**) but not in the shape of the terminal leaflets (**Figure 4; Table**
267 **1**), perhaps reflecting that tomato is inherently spirally phyllotactic and not all leaf features
268 reflect the transition to decussate phyllotaxy this mutation confers. Two different vine species,

bioRxiv preprint doi: https://doi.org/10.1101/043869; this version posted March 15, 2016. The copyright holder for this preprint (which was not certified by peer review) is the author/funder, who has granted bioRxiv a license to display the preprint in perpetuity. It is made available under aCC-BY-NC 4.0 International license.

common ivy and grapevine and its relatives, are statistically over-represented for opposite-signed leaf asymmetries compared to same-signed asymmetries (**Figure 5; Tables 2-3**), grapevine particularly so, again confirming the mirrored relationship predicted in the distichous model (**Figure 2F**).

Although we have focused on leaf shape, it is important to remember that auxin potentially impacts many more features of the leaf than just shape, or that leaf shape is a read-out of other underlying asymmetries at the cellular and tissue levels [15, 22, 23]. Further, it is possible that the patterning of auxin itself is influenced by properties specific to particular shoot apical meristem architectures. In this regard, it is important that the underlying developmental causes of leaf asymmetry be examined further. For example, the archetypal left-right leaf asymmetry of extreme midrib and blade curvature and spiraling seen in distichous *Begonia spp*. leaf pairs (**Figure 2G**) is apparent in very early primordia [24, 25]. In fact, in *Begonia* mirrored asymmetry appears to be the null condition, and symmetric *Begonia* have asymmetric primordia that become symmetric subsequently during development [24]. If leaf primordia are inherently asymmetric and symmetry is a result of secondary development, it is perhaps not so surprising that morphometric methods can statistically detect directional asymmetries in superficially symmetric species. We also note that the shoot apical meristem of grapevine and related species is dorsiventrally patterned perpendicular to the axis of distichous leaf initiation [26]. Different numbers of vascular traces enter the leaves on the dorsal and ventral sides of the shoot, which in the context of distichous phyllotaxy, creates an inherent mirrored asymmetry in vascular patterning, perhaps explaining the extremely strong mirrored asymmetry we observe in grapevine (**Table 3**).

bioRxiv preprint doi: https://doi.org/10.1101/043869; this version posted March 15, 2016. The copyright holder for this preprint (which was not certified by peer review) is the author/funder, who has granted bioRxiv a license to display the preprint in perpetuity. It is made available under aCC-BY-NC 4.0 International license.

Different phyllotactic systems—spiral, decussate, and distichous, among others—create inherently different spatial relationships between leaf primordia in the shoot apical meristem. The flux of auxin between leaf primordia especially accentuates differences along the left-right axis. Considering the global roles that auxin plays in vascular patterning and leaf shape, it is impressive that most leaves appear as bilaterally symmetric as they do. Our results clearly demonstrate that left-right leaf asymmetry, reflecting predicted auxin asymmetries in the shoot apical meristem, is influenced by phyllotaxy and present in diverse species.

MATERIALS AND METHODS

This work was conducted in parallel and together with our work on spiral phyllotaxy [5]. Some of the materials and methods from Chitwood, Headland et al., 2012 and Chitwood et al., 2016 are repeated here for convenience.

Plant Material and Growth and Conditions

Solanum lycopersicum accession LA3475 (cv. M82) was used for "wild-type" tomato measurements. The *entire-2* accession used for this study is 3-705. Tomato resources were obtained from the U.C. Davis Tomato Genetics Resource Center (TGRC). Tomato seed was sterilized for 2 minutes in 50% bleach, washed in water, and plated onto wet paper towels in Phytatrays (Sigma). Seed was kept at room temperature in darkness for 3 days and then transferred to chamber conditions in light for an additional three days before transplanting into Sunshine soil mix (Sun-Gro Horiculture). For measures of leaflet positioning and terminal leaflet shape, tomato plants were analyzed 33 days after plating seed.

bioRxiv preprint doi: https://doi.org/10.1101/043869; this version posted March 15, 2016. The copyright holder for this preprint (which was not certified by peer review) is the author/funder, who has granted bioRxiv a license to display the preprint in perpetuity. It is made available under aCC-BY-NC 4.0 International license.

316 Common ivy leaves (*Hedera helix*) were obtained from a single genotype of vine growing up
317 >6m walls enclosing a courtyard at the Donald Danforth Plant Science Center in St. Louis, MO
318 December 28, 2015. Documentation of the site location and material collected can be found in
319 the following link (https://twitter.com/DanChitwood/status/681554095618965504). The leaves
320 from 41 vines, with up to 25 leaves each, were dissected from the shoot and scanned.
321
322 Leaves from 20 different grapevine species and hybrids (*Vitis* and *Ampelopsis* spp.) were
323 collected from >270 vines in the USDA *Vitis* germplasm collection in Geneva, NY in June 2013
324 [20]. A single shoot was sampled from each vine, the leaves dissected, scanned, and their
325 position in the shoot noted.
326
327 ***Measures of lateral leaflet displacement and asymmetric shape***
328 Measurements of lateral leaflet position and terminal leaflet shape in tomato were made from
329 photographs. The first four leaves of tomato plants were dissected, placed under non-reflective
330 glass, and their terminal leaflets removed at the base. Photos of the leaf series were taken using
331 Olympus SP-500 UZ cameras mounted on copy stands (Adorama, 36'' Deluxe Copy Stand) and
332 controlled remotely by computer using Cam2Com software (Sabsik). Leaves from ivy and
333 grapevine were dissected from the shoot and scanned (Epson Workforce DS-50000, Suwa,
334 Japan). Care was taken to include the node position of each leaf in the scan.
335
336 In tomato, measures of the distance from the base of the terminal leaflet or the petiole to the most
337 distal and proximal leaflets were made using measurement functions in ImageJ. Lengths were
338 normalized using rulers present in each photograph. For shape analysis in tomato and ivy,

bioRxiv preprint doi: https://doi.org/10.1101/043869; this version posted March 15, 2016. The copyright holder for this preprint (which was not certified by peer review) is the author/funder, who has granted bioRxiv a license to display the preprint in perpetuity. It is made available under aCC-BY-NC 4.0 International license.

339 photographs were first converted to binary form using ImageJ and individual leaflets extracted
340 from the leaf series and named appropriately as separate files.
341
342 The analysis of tomato and ivy leaflet and leaf shape (respectively) was conducted using
343 Elliptical Fourier Descriptors followed by PCA using the program SHAPE [27]. Object contours
344 were extracted as chain-code. Chain-code was subsequently used to calculate normalized EFDs.
345 Normalization was based upon manual orientation with respect to the proximal-distal axis of the
346 leaflet/leaf. Principal component analysis was performed on the EFDs resulting from the first 20
347 harmonics of Fourier coefficients. Only asymmetric sources of shape variance were analyzed
348 using the *b* and *c* coefficients [28]. Coefficients of Elliptical Fourier Descriptors were calculated
349 at -2 and +2 standard deviations for each principal component and the respective contour shapes
350 reconstructed from an inverse Fourier transformation. PCs were then subsequently analyzed.
351
352 For grapevine data, 17 landmarks were placed, in order, for each leaf using the ImageJ [29] point
353 tool. Landmarks and their order were as follows: 1) petiolar junction, 2) midvein tip, 3) left distal
354 sinus, 4) right distal sinus, 5) left distal lobe tip, 6) right distal lobe tip, 7) left proximal sinus, 8)
355 right proximal sinus, 9) left proximal lobe tip, 10) right proximal lobe tip, 11) left terminus
356 petiolar vein, 12) right terminus petiolar vein, 13) branch point midvein, 14) branch point left
357 distal vein, 15) branch point right distal vein, 16) branch point left proximal vein, 17) branch
358 point right proximal vein (see Chitwood et al., 2016 for a visualization of landmark position).
359 Using ggplot2 [30] in R [31], graphs for landmarks from each image were visually checked for
360 errors. If errors were detected, the landmarking was redone for those particular samples. Once a
361 quality landmarked dataset was created, a Generalized Procrustes Analysis (GPA) was
362 undertaken using the R package shapes [32]. Eigenleaves were visualized using the shapepca

bioRxiv preprint doi: https://doi.org/10.1101/043869; this version posted March 15, 2016. The copyright holder for this preprint (which was not certified by peer review) is the author/funder, who has granted bioRxiv a license to display the preprint in perpetuity. It is made available under aCC-BY-NC 4.0 International license.

363 function and PC scores, percent variance explained by each PC, and Procrustes-adjusted
364 coordinates were obtained from procGPA object values.
365
366 *Statistical analysis*
367 All basic statistic functions were performed in R [31] and visualized in the package ggplot2 [30].
368 The cor.test() function in the stats package was used for all correlation analyses using method =
369 "pearson". Fisher's exact test was performed using fisher.test() and the one-way test used to
370 determine if the odds ratio of opposite-to-same orientations was greater than 1 by setting
371 alternative = "greater".
372
373 *Auxin transport modeling*
374 The simulation models have been described previously [5], however we summarize here for
375 completeness. Cells are modelled as polygons on a growing apex surface and thus are assumed to
376 be uniform in thickness. Extracellular space is ignored, and diffusion and transport occur directly
377 from cell to cell. The change in concentration of auxin in a cell is modeled as:

$$\begin{aligned} d[IAA_i] &= production - decay + diffusion + transport \\ &= \frac{\rho}{1+\kappa_{IAA}[IAA_i]} - \mu[IAA_i] + \frac{D}{A_i}\sum_{j\in N_i} l_{i\to j}([IAA_j]-[IAA_i]) \\ &\quad + \frac{T}{A_i}\sum_{j\in N_i}\left(PIN_{j\to i}\frac{b_T{}^{[IAA_j]}-1}{b_T{}^{[IAA_i]}} - PIN_{i\to j}\frac{b_T{}^{[IAA_i]}-1}{b_T{}^{[IAA_j]}}\right) \end{aligned} \quad (1)$$

378
379
380 where $[IAA_i]$ is the concentration of auxin in cell i, ρ controls the rate of production with
381 saturation coefficient κ_{IAA}, μ controls decay, D is the diffusion coefficient, A_i is the area of cell i,
382 N_i are the neighbours of cell i, $l_{i\to j}$ is the length of the wall between cell i and j, T is the transport
383 coefficient, $PIN_{i\to j}$ is the amount of PIN on the membrane of cell i facing cell j, and b_T is the
384 base for exponential transport. Equation (1) was used for the decussate simulation, but in the

bioRxiv preprint doi: https://doi.org/10.1101/043869; this version posted March 15, 2016. The copyright holder for this preprint (which was not certified by peer review) is the author/funder, who has granted bioRxiv a license to display the preprint in perpetuity. It is made available under aCC-BY-NC 4.0 International license.

385 distichous simulation we used the original quadratic transport term from Smith et al. (2006) [13]:

386

387 $$\frac{T}{A_i}\sum_{j\in N_i}\left(PIN_{j\to i}\frac{[IAA_j]^2}{[IAA_i]^2+\kappa_T}-PIN_{i\to j}\frac{[IAA_i]^2}{[IAA_j]^2+\kappa_T}\right) \quad (2)$$

388

389 where κ_T controls saturation of auxin transport. We model PIN allocation to the membranes as:
390

391 $$PIN_{i\to j}=[PIN_i]\frac{l_{i\to j}b_{PIN}{}^{[IAA_j]}}{\sum_{k\in N_i} l_{i\to k}b_{PIN}{}^{[IAA_k]}} \quad (3)$$

392

393 where $[PIN_i]$ is the total amount of PIN in cell i, and b_{PIN} is the base for exponential PIN

394 allocation to cell membrane sections. Equations (1-3) where implemented on the growing

395 cellular template as described in Smith et al. (2006) [13]. Simulations were performed using

396 Vertex-Vertex systems [33] in the Vlab modeling environment [34].

397

398 ACKNOWLEDGEMENTS

399 C.C.M was supported by a National Science Foundation Graduate Research Fellowship (DGE-

400 1148897), Katherine Esau Summer Fellowship, Walter R. and Roselinde H. Russell Fellowship,

401 and Elsie Taylor Stocking Fellowship. Part of the work was supported by NSF PGRP grant IOS–

402 0820854 (to N.R.S., Julin Maloof and Jie Peng). Funding for R.S.S. was provided by the

403 SystemsX.ch Plant Growth Research, Technology, and Development project and the Max Planck

404 Society.

405

406 AUTHOR CONTRIBUTIONS

407 C.C.M, D.H.C, R.S.S, & N.R.S designed the experiments, performed the experiments, analyzed

408 the data and wrote the paper.

409

410 FIGURE AND TABLE LEGENDS

bioRxiv preprint doi: https://doi.org/10.1101/043869; this version posted March 15, 2016. The copyright holder for this preprint (which was not certified by peer review) is the author/funder, who has granted bioRxiv a license to display the preprint in perpetuity. It is made available under aCC-BY-NC 4.0 International license.

411 **Figure 1: Leaf morphology is defined by four axes and the position of the leaf is defined by**
412 **phyllotaxis. A**) Schematic describing three developmental axes of a leaf. The medio-lateral axis
413 describes the mid-vein to margin region of a leaf. The adaxial-abaxial axis defines the top and
414 bottom of the leaf, respectively. The distal-proximal axis refers to the leaf tip relative to the base.
415 **B-C**) The descending and ascending axis of a leaf refers to the left and right sides of the leaf in
416 relation to spiral phyllotactic patterning. Spiral phyllotaxy can be further defined as Clockwise
417 (C) or Counter-Clockwise (CC). The ascending side of the leaf faces the direction of younger
418 leaves, while the descending side faces older leaves. **D**) When the divergence angle between
419 each leaf is ~137.5˚ the phyllotaxis is defined as spiral. Decussate phyllotaxis refers to leaf
420 initiation patterning where leaves initiate in pairs 180˚ apart, with 90˚ between each successive
421 pair (literally "crossed"). **F**) Distichous phyllotaxis occurs when leaves initiate one at a time
422 180˚apart (literally "of two rows").
423
424 **Figure 2: Models of decussate and distichous phyllotaxis predict reflection within leaf**
425 **pairs.** A) Pairs of leaves from decussate and distichous phyllotactic simulations were analyzed
426 such that all pairs have positive divergence angles. IAA Shift values in auxin concentration are
427 then analyzed for "primordium A" and "primordium B" as indicated in purple and blue dotted
428 lines, respectively. Sign (+ or -) and direction (C, clockwise and CC, counter-clockwise) of IAA
429 Shift values are as indicated. **B-C**) Diagrams demonstrating the relative mirrored relationships
430 between primordia pairs if IAA Shift values share the same sign and direction (B, "pinwheel,"
431 ++ or --) or are opposite in sign (C, "mirror," +- or -+). **D-F**) As divergence angles deviate from
432 180˚ and become smaller, auxin peak concentrations remain truer to an idealized 180˚ angle. As
433 the divergence angle decreases, primordium A IAA Shift values decrease, whereas IAA Shift

bioRxiv preprint doi: https://doi.org/10.1101/043869; this version posted March 15, 2016. The copyright holder for this preprint (which was not certified by peer review) is the author/funder, who has granted bioRxiv a license to display the preprint in perpetuity. It is made available under aCC-BY-NC 4.0 International license.

values increase under similar conditions for primordium B, such that the discrepancy between auxin and primordia center of masses are mirrored between the two primordia. Results from **D**) decussate and **F**) distichous models are shown, as well as **E**) an image from the decussate model showing primordia (white) and auxin (green) center of masses. **G**) *Begonia* species are excellent examples of reflected, mirrored leaf morphology between distichous leaf pairs, which sometimes manifests as a spiral morphology (lower panel).

Figure 3: The decussate-like mutant *e-2*. A) Relative to a WT background genotype, *entire-2* (*e-2*) exhibits decussate-like phyllotactic patterning. Leaflets have been removed to better view divergence angles. B) Between leaf pairs 1/2 and 3/4 *e-2* divergence angles more closely approximate 180˚ compared to background genotype. C) "L" and "R" depict the lengths measured to analyze shifts in lateral leaflet positioning on leaf 1 ($L_1 - R_1$) and leaf 2 ($L_2 - R_2$). D) Lateral leaflets on the left and right sides of leaves show a significant negative correlation in the lateral leaflet positioning between leaves 1 and 2, indicative of a mirrored relationship between leaf pairs.

Figure 4: Morphometric analysis of *e-2* terminal leaflets. A) Distal bulges in terminal leaflet laminae in the *e-2* mutant background occur either on opposite sides of leaf 1/2 pairs or on the same side. B) Principal Components (PCs) representing asymmetric shape variance using Elliptical Fourier Descriptors (EFDs). Negative PC standard deviation values are of opposite asymmetric orientation compared to positive values. Percent asymmetric shape variance explained by each PC is provided.

bioRxiv preprint doi: https://doi.org/10.1101/043869; this version posted March 15, 2016. The copyright holder for this preprint (which was not certified by peer review) is the author/funder, who has granted bioRxiv a license to display the preprint in perpetuity. It is made available under aCC-BY-NC 4.0 International license.

457 **Figure 5: Morphometric analysis of ivy and grapevine leaves.** A) An example of leaf outlines
458 analyzed from a shoot of common ivy (*Hedera helix*). Shoot tip and base are indicated. B)
459 Principal Components (PCs) representing asymmetric shape variance using Elliptical Fourier
460 Descriptors (EFDs). Negative PC standard deviation values are of opposite asymmetric
461 orientation compared to positive values. Percent asymmetric shape variance explained by each
462 PC is provided. C) An example of leaf outlines analyzed from a grapevine shoot (specifically,
463 *Vitis xdoaniana*, for which each of the nine leaf pairs have an opposite orientation, see **Table 4**).
464 The analyzable leaf pairs for a shoot equals n-1, where n = total leaf number. In this study, 20
465 different *Vitis* and *Ampelopsis* (a closely-related genus to *Vitis*) species and hybrids were
466 analyzed. D) PCs representing shape variance in 17 Procrustes-adjusted homologous landmarks.
467 Note that almost all asymmetric shape variance is restricted to PC4, explaining 10.5% of total
468 shape variance, which is analyzed in **Table 4**.
469
470 **Figure 6: Summary of leaf asymmetry in spiral, decussate, and distichous systems.** The
471 discrepancy between the peak concentration of auxin (blue) and the respective primordium
472 center of mass (black) is such that the auxin falls towards a more idealized phyllotactic position.
473 In both A) spiral and B-D) decussate/distichous systems, this results in the distal shifting of
474 morphological features (such as leaflets, terminal leaflet lobes) and increase laminar outgrowth
475 on the side of the primordium with greater auxin concentration. Asymmetries early in leaf
476 development manifest as the shifting of distal features on the descending side of mature leaves in
477 spiral systems and mirroring of leaf features in decussate/distichous systems.
478
479 **Table 1: Opposite vs. same orientation in *e-2* leaf1/leaf2 pairs**

bioRxiv preprint doi: https://doi.org/10.1101/043869; this version posted March 15, 2016. The copyright holder for this preprint (which was not certified by peer review) is the author/funder, who has granted bioRxiv a license to display the preprint in perpetuity. It is made available under aCC-BY-NC 4.0 International license.

PC	Variance	Opposite	Same	n	Ratio	p value
PC1	52.0%	89	94	183	0.95	0.64
PC2	13.6%	87	96	183	0.91	0.72
PC3	9.1%	80	103	183	0.78	0.91
PC4	4.8%	89	94	183	0.95	0.64

For each PC representing asymmetric shape variance in the terminal leaflets of *e-2* (**Figure 4B**), the number of leaflet pairs with opposite vs. same PC sign, the number of leaf pairs, the ratio of the number of opposite-to-same pairs, and the p-value for the one-sided exact test that the odds ratio of opposite-to-same pairs exceeds 1 are provided.

Table 2: Opposite vs. same orientation in common ivy (*Hedera helix*) leaf pairs

PC	Variance	Opposite	Same	n	Ratio	p value
PC1	61.1%	430	394	824	1.09	0.2011
PC2	11.4%	462	362	824	1.28	0.0078
PC3	9.8%	451	373	824	1.21	0.0304
PC4	5.2%	437	387	824	1.13	0.1184

For each PC representing asymmetric shape variance in ivy leaves (**Figure 5B**), the number of leaf pairs with opposite vs. same PC sign, the number of leaf pairs, the ratio of the number of opposite-to-same pairs, and the p-value for the one-sided exact test that the odds ratio of opposite-to-same pairs exceeds 1 are provided.

bioRxiv preprint doi: https://doi.org/10.1101/043869; this version posted March 15, 2016. The copyright holder for this preprint (which was not certified by peer review) is the author/funder, who has granted bioRxiv a license to display the preprint in perpetuity. It is made available under aCC-BY-NC 4.0 International license.

491

492 **Table 3: Opposite vs. same orientation in grapevine (*Vitis* and *Ampelopsis* spp.) leaf pairs**

493

Species	Opposite	Same	n	Ratio	p value
Vitis riparia	646	197	843	3.28	2.20E-16
Vitis labrusca	287	96	383	2.99	6.01E-13
Vitis cinerea	268	92	360	2.91	8.40E-12
Vitis rupestris	201	102	303	1.97	3.08E-05
Vitis acerifolia	165	44	209	3.75	3.85E-10
Vitis amurensis	146	61	207	2.39	1.40E-05
Unidentified *Vitis spp.*	143	59	202	2.42	1.41E-05
Vitis vulpina	108	47	155	2.30	0.0002962
Vitis aestivalis	70	26	96	2.69	0.0008781
Vitis coignetiae	37	21	58	1.76	0.09458
Ampelopsis glandulosa	38	9	47	4.22	0.001473
Vitis palmata	27	18	45	1.50	0.2274
Vitis xchampinii	26	6	32	4.33	0.008431
Vitis piasezkii	15	9	24	1.67	0.2806
Ampelopsis cordata	6	5	11	1.20	0.5789
Vitis thunbergii	6	5	11	1.20	0.5789
Vitis xandersonii	9	1	10	9.00	0.07043
Ampelopsis	4	5	9	0.80	0.7578

bioRxiv preprint doi: https://doi.org/10.1101/043869; this version posted March 15, 2016. The copyright holder for this preprint (which was not certified by peer review) is the author/funder, who has granted bioRxiv a license to display the preprint in perpetuity. It is made available under aCC-BY-NC 4.0 International license.

aconitifolia					
Vitis xdoaniana	9	0	9	Inf	0.02167
Vitis xnovae-angliae	5	2	7	2.50	0.3776

For different *Vitis* and *Ampelopsis* species, and *Vitis* hybrids, the number of leaf pairs with opposite vs. same PC4 sign (**Figure 5D**), the number of leaf pairs, the ratio of the number of opposite-to-same pairs, and the p-value for the one-sided exact test that the odds ratio of opposite-to-same pairs exceeds 1 are provided.

REFERENCES

1. Miller AP (1995) Leaf-Mining Insects and Fluctuating Asymmetry in Elm Ulmus glabra Leaves. J Anim Ecol 64:697–707

2. Kozlov MV, Wilsey BJ, Koricheva J, Haukioja E (1996) Fluctuating Asymmetry of Birch Leaves Increases Under Pollution Impact. J Appl Ecol 33:1489–1495

3. Hódar JA (2002) Leaf fluctuating asymmetry of Holm oak in response to drought under contrasting climatic conditions. J Arid Environ 52:233–243

4. Klingenberg C (2015) Analyzing Fluctuating Asymmetry with Geometric Morphometrics: Concepts, Methods, and Applications. Symmetry 7:843–934

5. Chitwood DH, Headland LR, Ranjan A, Martinez CC, Braybrook S a., Koenig DP, Kuhlemeier C, Smith RS, Sinha NR (2012) Leaf Asymmetry as a Developmental Constraint Imposed by Auxin-Dependent Phyllotactic Patterning. Plant Cell 24:1–10

6. Chitwood DH, Naylor DT, Thammapichai P, Weeger ACS, Headland LR, Sinha NR (2012) Conflict between Intrinsic Leaf Asymmetry and Phyllotaxis in the Resupinate Leaves of Alstroemeria psittacina. Front Plant Sci 3:182

7. Korn RW (2006) Anodic asymmetry of leaves and flowers and its relationship to phyllotaxis. Ann Bot 97:1011–1015

8. Skutch AF (1927) Anatomy of Leaf of Banana, Musa sapientum L. var. Hort. Gros Michel. Bot Gaz 84:337–391

9. Macloskie G (1895) Antidromy in Plants. Am Nat 29:973–978

bioRxiv preprint doi: https://doi.org/10.1101/043869; this version posted March 15, 2016. The copyright holder for this preprint (which was not certified by peer review) is the author/funder, who has granted bioRxiv a license to display the preprint in perpetuity. It is made available under aCC-BY-NC 4.0 International license.

519 10. Raunkiær C (1919) Über Homodromie und Antidromie insbesondere bei Gramineen. Andr.
520 Fred. Høst & søn, Bianco Lunos bogtrykkeri

521 11. Dormer KJ (1972) Shoot Organization in Vascular Plants. Syracuse University Press

522 12. Reinhardt D, Pesce E-R, Stieger P, Mandel T, Baltensperger K, Bennett M, Traas J, Friml
523 J, Kuhlemeier C (2003) Regulation of phyllotaxis by polar auxin transport. Nature
524 426:255–260

525 13. Smith RS, Guyomarc'h S, Mandel T, Reinhardt D, Kuhlemeier C, Prusinkiewicz P (2006)
526 A plausible model of phyllotaxis. Proc Natl Acad Sci U S A 103:1301–1306

527 14. Scarpella E, Barkoulas M, Tsiantis M (2010) Control of leaf and vein development by
528 auxin. Cold Spring Harb Perspect Biol 2:a001511

529 15. Koenig D, Bayer E, Kang J, Kuhlemeier C, Sinha N (2009) Auxin patterns Solanum
530 lycopersicum leaf morphogenesis. Development 136:2997–3006

531 16. Martinez C, Koenig D, Chitwood DH, Sinha N (2016) A Sister of PIN1 gene in tomato
532 (Solanum lycopersicum) defines organ initiation patterns by maintaining epidermal auxin
533 flux. bioRxiv 042150

534 17. Jönsson H, Heisler MG, Shapiro BE, Meyerowitz EM, Mjolsness E (2006) An auxin-
535 driven polarized transport model for phyllotaxis. Proc Natl Acad Sci U S A 103:1633–1638

536 18. Smith RS (2011) Modeling plant morphogenesis and growth. New Trends in the Physics
537 and Mechanics of Biological Systems

538 19. Giulini A, Wang J, Jackson D (2004) Control of phyllotaxy by the cytokinin-inducible
539 response regulator homologue ABPHYL1. Nature 430:1031–1034

540 20. Chitwood DH, Klein LL, O'Hanlon R, Chacko S, Greg M, Kitchen C, Miller AJ, Londo JP
541 (2016) Latent developmental and evolutionary shapes embedded within the grapevine leaf.
542 New Phytol 210:343–355

543 21. Dormer KJ, Hucker J (1957) Observations on the Occurrence of Prickles on the Leaves of
544 Ilex aquifolium. Ann Bot 21:385–398

545 22. Barkoulas M, Hay A, Kougioumoutzi E, Tsiantis M (2008) A developmental framework
546 for dissected leaf formation in the Arabidopsis relative Cardamine hirsuta. Nat Genet
547 40:1136–1141

548 23. Shani E, Ben-Gera H, Shleizer-Burko S, Burko Y, Weiss D, Ori N (2010) Cytokinin
549 regulates compound leaf development in tomato. Plant Cell 22:3206–3217

550 24. Barabé D, Brouillet L, Bertrand C (1992) Organogénie de la feuille du Begonia radicans

bioRxiv preprint doi: https://doi.org/10.1101/043869; this version posted March 15, 2016. The copyright holder for this preprint (which was not certified by peer review) is the author/funder, who has granted bioRxiv a license to display the preprint in perpetuity. It is made available under aCC-BY-NC 4.0 International license.

551 Vellozo et du Begonia scabrida (Begoniaceae). Can J Bot 70:1107–1122

552 25. Charlton WA (1993) The rotated-lamina syndrome. III. Cases in Begonia, Corylus,
553 Magnolia, Pellionia, Prunus, and Tilia. Can J Bot 71:229–247

554 26. Gerrath J m., Posluszny U, Dengler N g. (2001) Primary Vascular Patterns in the Vitaceae.
555 Int J Plant Sci 162:729–745

556 27. Iwata H, Ukai Y (2002) SHAPE: a computer program package for quantitative evaluation
557 of biological shapes based on elliptic Fourier descriptors. J Hered 93:384–385

558 28. Iwata H, Niikura S, Matsuura S, Takano Y, Ukai Y Evaluation of variation of root shape of
559 Japanese radish (Raphanus sativus L.) based on image analysis using elliptic Fourier
560 descriptors. Euphytica 102:143–149

561 29. Abràmoff MD, Magalhães PJ, Ram SJ (2004) Image processing with ImageJ. Biophotonics
562 international 11:36–42

563 30. Wickham H (2009) ggplot2: elegant graphics for data analysis. Springer Science &
564 Business Media

565 31. Team RC (2014) A language and environment for statistical computing. R Foundation for
566 Statistical Computing, Vienna.

567 32. Dryden IL (2013) shapes: Statistical shape analysis. R package version 1.1-1.

568 33. Smith RS, Schuepbach T, Nakayama N (2004) MorphoGraphX : A Program for
569 Quantitative Analysis of Tissue Kinematics and Fluorescence Expression Using 2D
570 Surface Projections. Growth 2004

571 34. Federl P, Prusinkiewicz P (1999) Virtual Laboratory: An Interactive Software Environment
572 for Computer Graphics. In: Computer Graphics International. p 93-100

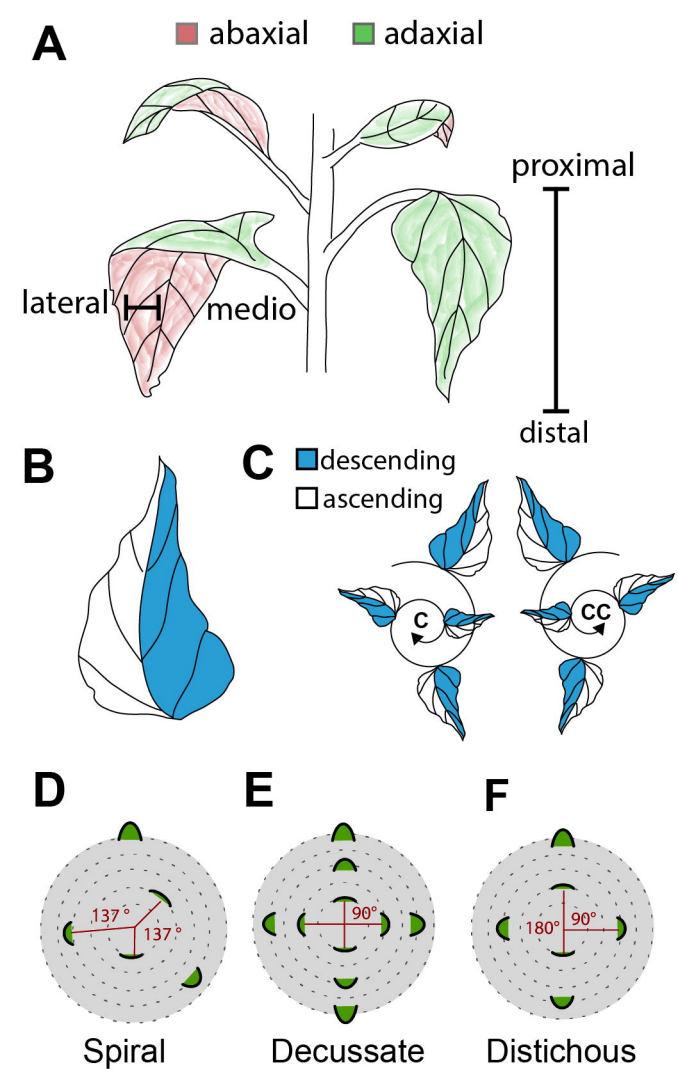
A
abaxial
adaxial
proximal
distal
lateral
medio
B
C
descending
ascending
C
CC
D
137 °
137 °
Spiral
E
90°
Decussate
F
180°
90°
Distichous

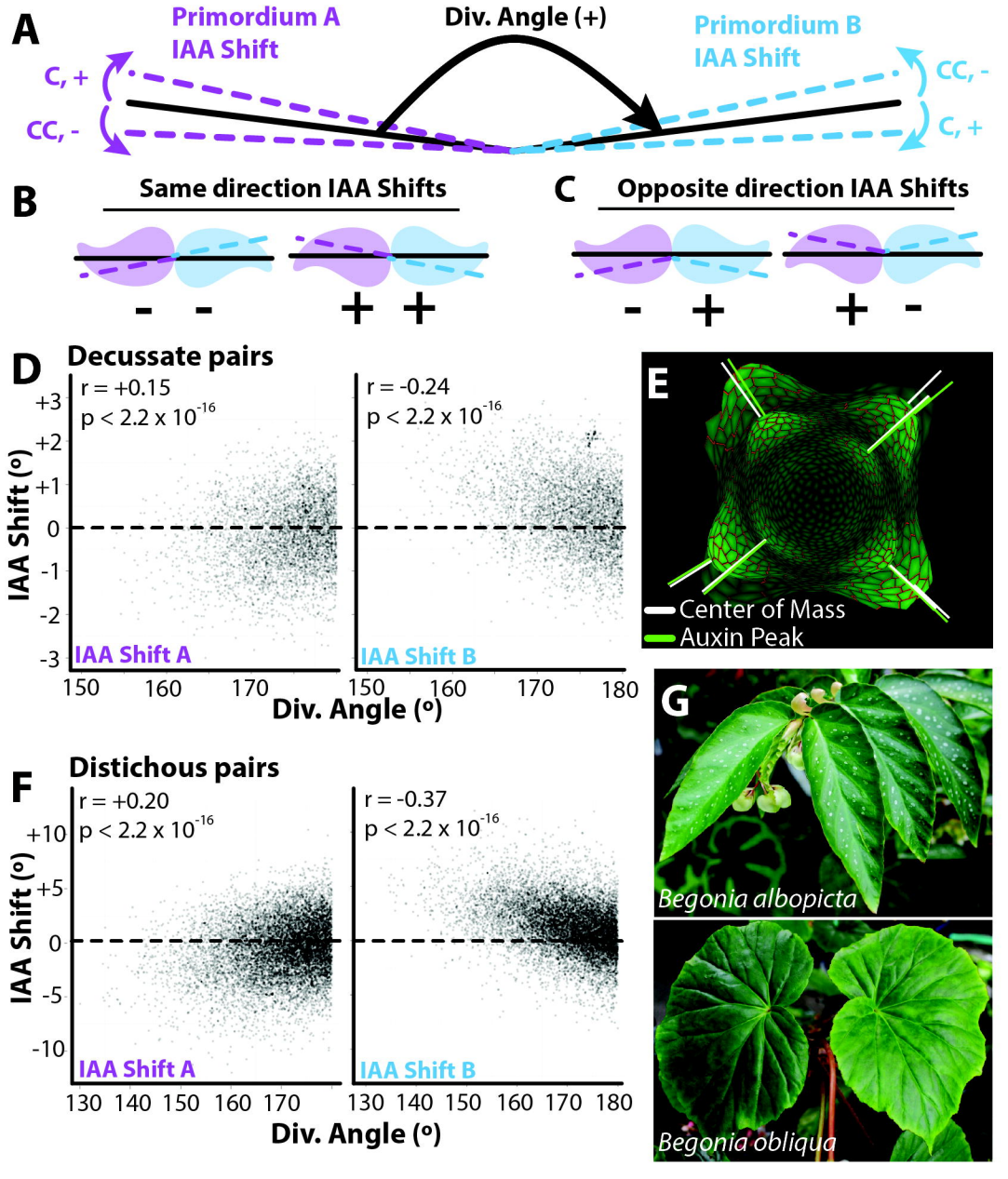
A
Primordium A
IAA Shift
Div. Angle (+)
Primordium B
IAA Shift
C, +
CC, -
CC, -
C, +
B
Same direction IAA Shifts
- -
+ +
C
Opposite direction IAA Shifts
- +
+ -
D
Decussate pairs
r = +0.15
p < 2.2 x 10-16
r = -0.24
p < 2.2 x 10-16
IAA Shift (°)
+3
+2
+1
0
-1
-2
-3
IAA Shift A
IAA Shift B
150 160 170
150 160 170 180
Div. Angle (°)
E
Center of Mass
Auxin Peak
F
Distichous pairs
r = +0.20
p < 2.2 x 10-16
r = -0.37
p < 2.2 x 10-16
IAA Shift (°)
+10
+5
0
-5
-10
IAA Shift A
IAA Shift B
130 140 150 160 170
130 140 150 160 170 180
Div. Angle (°)
G
Begonia albopicta
Begonia obliqua

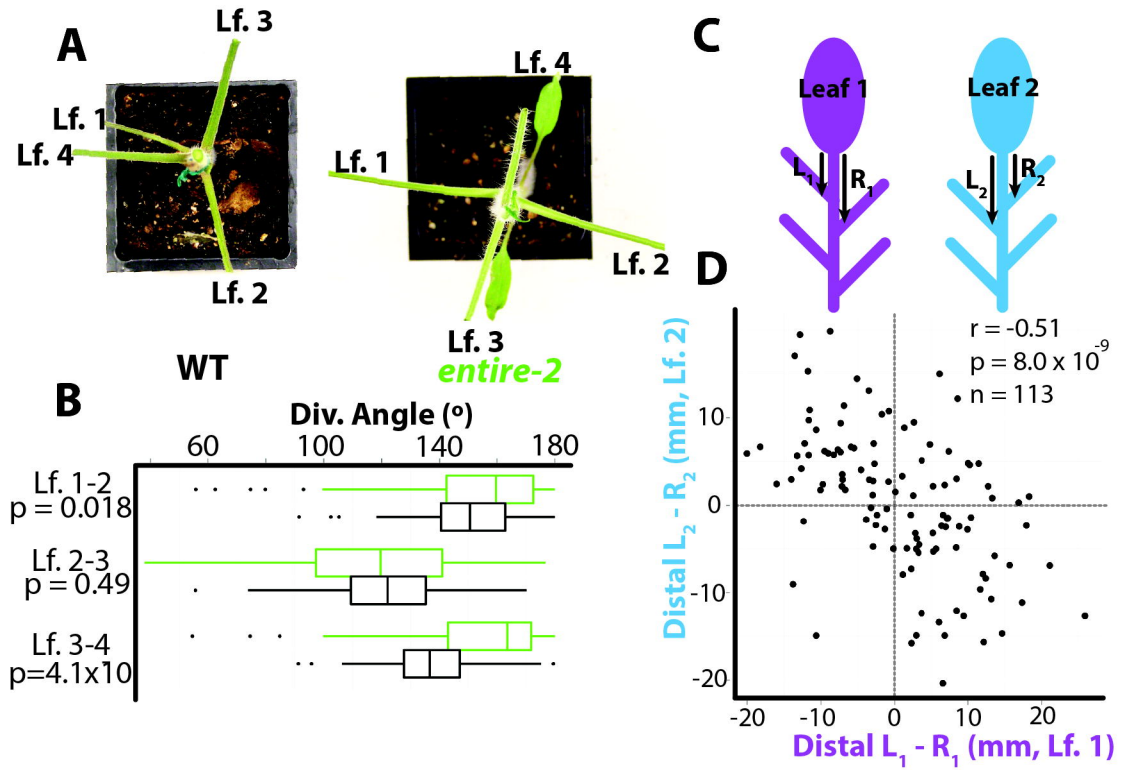
A
Lf. 3
Lf. 1
Lf. 4
Lf. 2
Lf. 4
Lf. 1
Lf. 2
Lf. 3
WT
entire-2
B
Div. Angle (°)
60
100
140
180
Lf. 1-2
p = 0.018
Lf. 2-3
p = 0.49
Lf. 3-4
p=4.1x10
C
Leaf 1
Leaf 2
L1
R1
L2
R2
D
r = -0.51
p = 8.0 x 10-9
n = 113
Distal L2 - R2 (mm, Lf. 2)
Distal L1 - R1 (mm, Lf. 1)
10
0
-10
-20
-20
-10
0
10
20

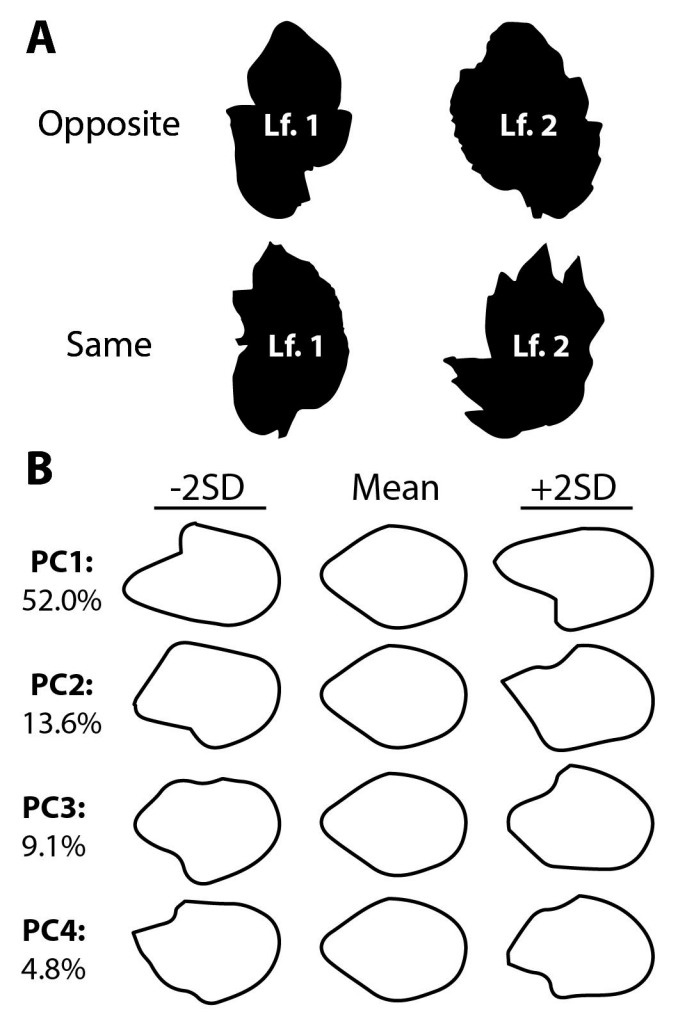
A
Opposite
Lf. 1
Lf. 2
Same
Lf. 1
Lf. 2
B
-2SD
Mean
+2SD
PC1:
52.0%
PC2:
13.6%
PC3:
9.1%
PC4:
4.8%

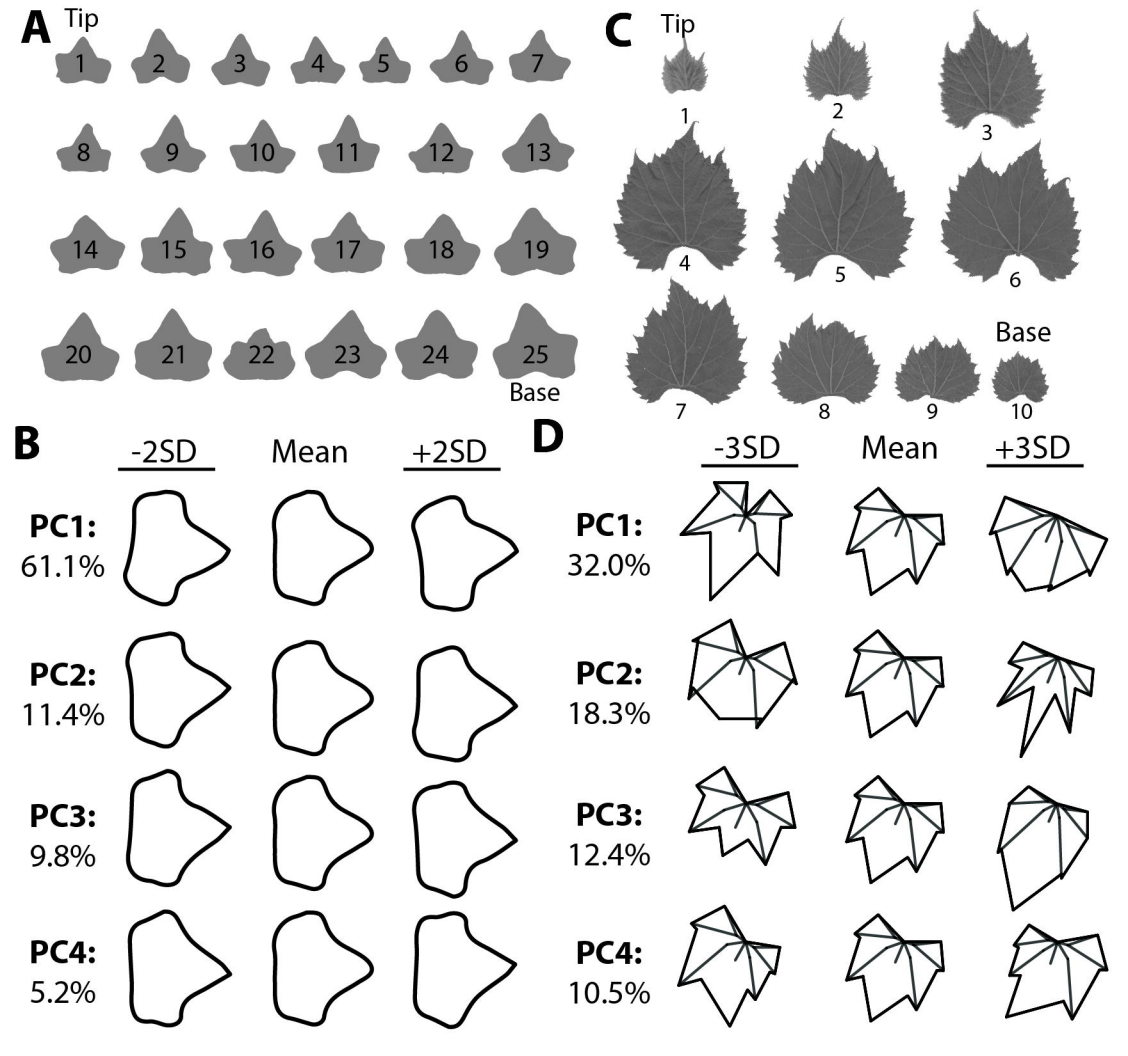
A
Tip
1
2
3
4
5
6
7
8
9
10
11
12
13
14
15
16
17
18
19
20
21
22
23
24
25
Base
C
Tip
1
2
3
4
5
6
7
8
9
10
Base
B
-2SD
Mean
+2SD
PC1:
61.1%
PC2:
11.4%
PC3:
9.8%
PC4:
5.2%
D
-3SD
Mean
+3SD
PC1:
32.0%
PC2:
18.3%
PC3:
12.4%
PC4:
10.5%

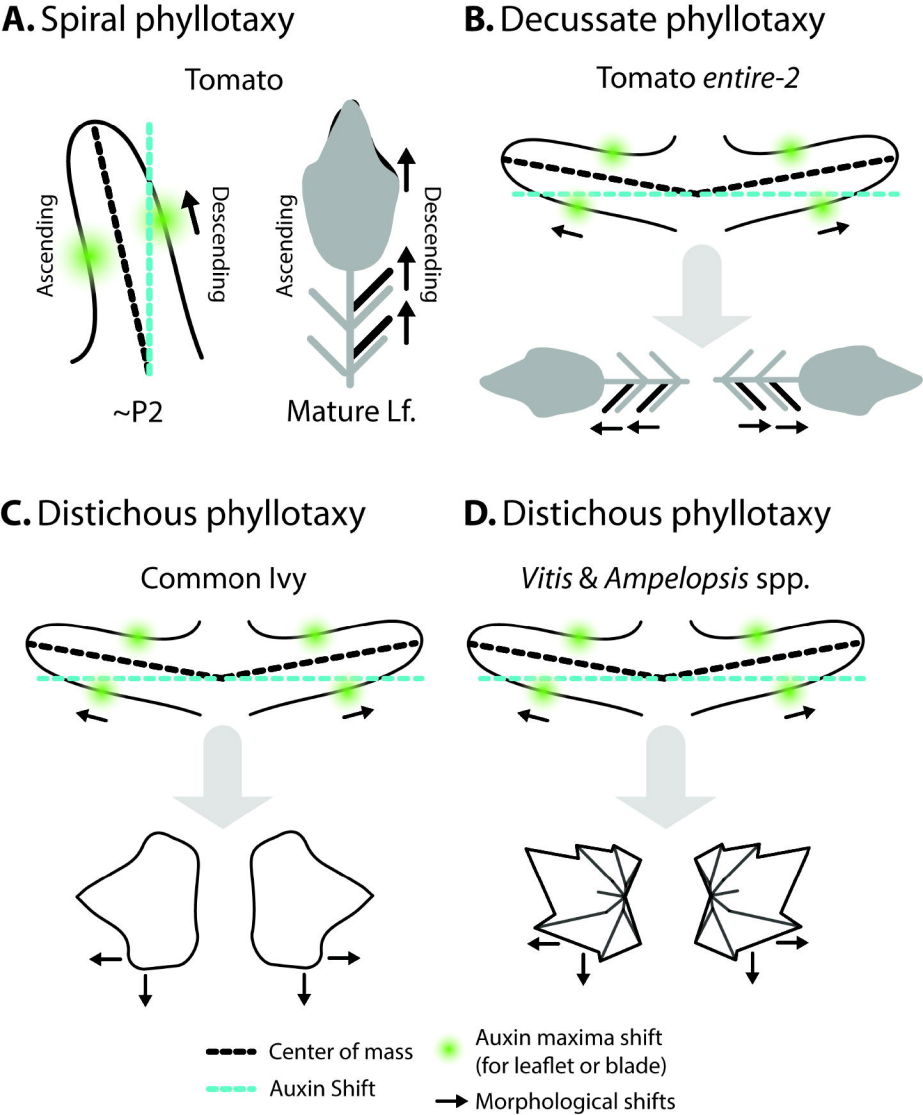
A. Spiral phyllotaxy
Tomato
Ascending
Descending
~P2
Ascending
Descending
Mature Lf.
B. Decussate phyllotaxy
Tomato entire-2
C. Distichous phyllotaxy
Common Ivy
D. Distichous phyllotaxy
Vitis & Ampelopsis spp.
Center of mass
Auxin Shift
Auxin maxima shift
(for leaflet or blade)
Morphological shifts